JOURNAL OF ELECTROMAGNETIC ENGINEERING AND SCIENCE, VOL. 20, NO. 2, 115~124, APR. 2020

https://doi.org/10.26866/jees.2020.20.2.115
ISSN 2671-7263 (Online) · ISSN 2671-7255 (Print)

Miniature Slotted Semi-Circular Dual-Band Antenna for WiMAX and WLAN Applications

Dhirgham Kamal Naji*

Abstract

In this paper, a new approach is presented for designing a miniaturized microstrip patch antenna (MPA) for dual-band applications. The proposed MPA consists of a semi-circular patch radiator fed by a 50-Ω coplanar waveguide (CPW) structure with a tapered-ground plane for enhancing impedance bandwidth over the dual-band. By inserting a folded U-shaped slot into the semi-circular patch, the proposed antenna introduces an additional higher-order mode but does not modify the resonance frequency of the lower-order mode of the patch, yielding the desired dual-band response. For antenna miniaturization, the circular-shaped radiator of the reference antenna (RA) was converted into a semi-circular radiating patch. Agreement between CST and HFSS simulated results led us to manufacture a prototype of the designed antenna on one side of an inexpensive FR-4 substrate with an overall dimension of $17 \times 18 \times 0.8$ mm^3. The measured result in terms of reflection coefficient S_{11} confirms that the antenna operates in both 3.5 GHz (3.4–3.7 GHz) and 5.8 GHz (5.725–5.875 GHz) bands suitable for use in WiMAX and WLAN applications, respectively. Moreover, besides an area reduction of 32% compared with the RA counterpart, the proposed antenna has other features, a simple geometry, and is easy to manufacture in comparison with previously reported antenna structures.

Key Words: Circular Microstrip Patch Antenna, Coplanar Waveguide, Semi-Circular Patch, Semi-Circular Slotted Antenna.

I. Introduction

In recent years, remarkable interest has been generated in antennas characterized by a miniaturize size and the potential to operate at different frequency bands suitable for modern wireless communication systems, such as radio frequency identification (RFID), wireless local area networks (WLAN), and worldwide interoperability for microwave access (WiMAX). Thus, multi-band antennas should operate in the desired frequency bands allocated for these applications: 2.45 GHz (2.4–2.5 GHz), 5.8 GHz (5.725–5.875 GHz), and 3.5 GHz (3.4–3.7 GHz), respectively. In order to meet these requirements, in addition to meeting the widespread demand for antennas that are light-weight, low-cost, and easy to fabricate, microstrip antennas represent the best solution for use in most applications [1–8].

It is well known that designing a miniaturized antenna for dual-band or multi-band applications is a difficult task, with several attempts to do so already reported in the literature [9–13]. In these papers, many techniques for designing dual-band antennas that cover WLAN and WiMAX bands were successfully demonstrated, like using shorting pins [9], employing a rectangular-shaped strip ring along with a defected ground structure [10], implementing fractal-shaped geometry [11, 12], or designing a 9-pointed-star monopole antenna [13]. In addition, a circular ring [14] and two arc-shaped strips [15] with a slot in their ground were successfully designed to satisfy the specifications of

Manuscript received November 10, 2019 ; Revised January 11, 2020 ; Accepted January 28, 2020. (ID No. 20191110-095J)
Electronic and Communications Engineering Department, College of Engineering, Al-Nahrain University, Baghdad, Iraq.
*Corresponding Author: Dhirgham Kamal Naji (e-mail: dknaji73@yahoo.com)

the 2.4/2.5 GHz WiMAX/WLAN and 3.5/5.5 GHz WiMAX bands.

In recent years, researchers have mostly used a coplanar waveguide (CPW) mechanism to feed their proposed antennas because of its attractive features, such as a simple feeding structure, a wider impedance bandwidth with good radiation characteristics, and easy integration with passive and active devices [16–18]. For instance, in literature [19, 20], new ideas were demonstrated for designing compact, CPW-fed microstrip antennas with dual-band characteristics. In [19], a novel approach was proposed for designing a compact-size (20×22 mm^2) microstrip antenna with dual-band characteristics for 3.5-GHz WLAN and 5.5-GHz WiMAX band systems. This proposed antenna uses a grounded CPW mechanism for feeding the antenna, and two strip-shaped patch radiators to maintain 3.5 GHz and 5.5 GHz. When using only one strip, the lower resonant frequency at 3.5 GHz is excited with a frequency band at 3.06–3.89 GHz, while another resonant frequency at 5.8 GHz with a frequency band at 5.14–5.93 GHz is achieved by the antenna when the other arm is included. A planar meandered line monopole antenna with a fork- and double fork-shaped strip were presented in [20] for the design scheme of compact antennas with a size of 21×21 mm^2 and improved dual-band performance for 3.5- and 5.5-GHz wireless applications.

Due to their interesting features, metamaterials have been reported by researchers for antenna miniaturization and multiband applications. For instance, a folded monopole dual-band antenna [21] consisting of a composite right- and left-handed metamaterial was proposed for 2.5- and 5.8-GHz center frequencies (from the normal strip and a single metamaterial cell, respectively), which can be controlled independently by varying their geometrical parameters. Although the above techniques have achieved remarkable success in designing antennas with the potential for operating within multiple frequency bands, most of these antennas have large dimensions or a complex structure, or they are difficult to manufacture.

Unlike the previous dual-band antennas mentioned above, the present proposed antenna meets the requirements of WiMAX and WLAN devices. Therefore, it is useful to introduce a two-band, semi-circular-shaped monopole antenna with a simple miniature structure that enables the independent tuning of the two bands. This issue is addressed here.

In this paper, a semi-circular slotted antenna (SCSA) is described. The conventional semi-circular patch is loaded with a folded U-slot structure to achieve dual-band characteristics and 3.5-GHz WiMAX and 5.8-GHz WLAN bands. An impedance bandwidth over the dual-band frequency spectrum is obtained by feeding the radiating patch by a CPW feedline mechanism. The proposed antenna structure is created by using a finite integration method-based CST Microwave Studio simulator to confirm the results, Ansoft's finite element technique-based High-Frequency Structure Simulator (HFSS) was used. To validate the simulated results, the prototype antenna structure was fabricated, and good agreement was achieved between the experimental and simulated results. The designed antenna has a miniaturized size, a simple structure, and is easy to manufacture in comparison with previously reported antenna structures.

II. Design Concepts of the Dual-Band Antenna

This section describes the geometry of a miniaturized dual-band antenna structure and outlines the four basic steps of the procedure applied to the designed antenna. The concept of a folded U-shaped loaded structure to achieve a miniaturized dual-band antenna is presented here. Initially, the design procedure begins with a conventional reference antenna, which is inset-fed with a circular microstrip patch antenna (CMPA). Then, intermediate design steps are successively applied to achieve an SCSA with a size reduction of 32% compared with the reference antenna.

1. Antenna Geometry

The geometry of the proposed antenna is shown in Fig. 1. The semi-circular patch antenna's radiator of radius R is etched on the top side of one side of an FR4 glass epoxy substrate of dimensions $L_{sub} \times W_{sub}$ (17 mm $\times$ 18 mm); its other parameters are as follows: a substrate height of $h_{sub} = 0.8$ mm, a dielectric constant of $\varepsilon_r = 4.4$, a loss tangent $tan\ of\ \delta = 0.025$, and a conductor thickness of 35 μm. The feed conductor of the CPW structure of length L_f is connected to the center of the semi-circular patch, and the CPW feed width W_f and gap g are calculated using CST MWS to yield a characteristic impedance of 50 Ω. The calculated CPW dimensions are $W_f = 2.0$ mm and $g = 0.25$ mm. Two symmetrically tapered ground planes for bandwidth enhancement with a length of L_g are placed at distance g around the CPW feedline. A folded U-shaped slot structure (large and short widths, w_1 and w_2, respectively, length l_1 and thickness t) is cut at distance d from the semi-circular patch.

An SMA connector is used for correctly modeling the proposed antenna in CST and HFSS simulators in order to account for its effect on the result, and a waveguide port is used to feed the antenna. All metallic conductors used for simulating the designed antenna, depicted as brown in Fig. 1, are chosen as a perfect electric conductor (PEC). Table 1 lists the optimized geometrical dimensions of the proposed antenna.

2. Design Details

The design concept is introduced here for a reference antenna

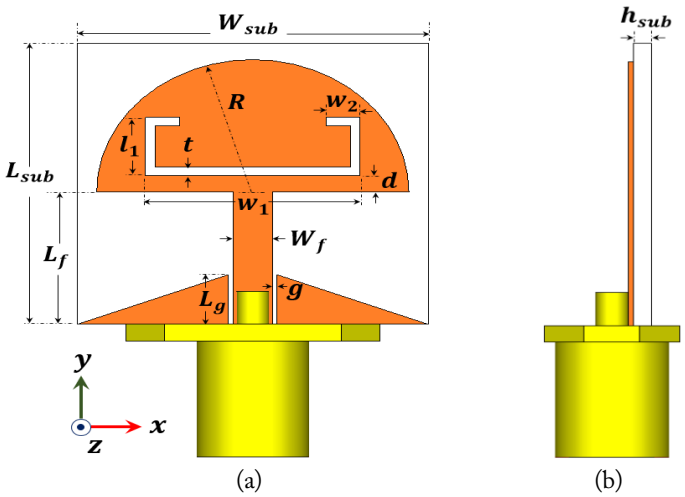

(a) (b)

Fig. 1. Geometry of the proposed antenna: (a) front view and (b) side view.

Table 1. Geometric parameters of the proposed antenna

Geometric parameter	Symbol	Value (mm)
Substrate length	L_{sub}	17.0
Substrate width	W_{sub}	18.0
Substrate height	h_{sub}	0.8
Patch radius	R	8.0
CPW-fed width	W_f	2.0
CPW-fed length	L_f	8.0
CPW-fed gap	g	0.25
The major width of U-slot	w_1	11.0
The length of U-slot	l_1	3.0
The minor width of U-slot	w_2	1.75
The thickness of U-slot	t	0.5
The location distance of U-slot	d	1.0

(RA) with a circular-shaped patch configuration, and the design steps can also be applied for other patch geometries. Thus, a circular patch was chosen as an RA in this work, as it offers a minimum footprint area in the final antenna compared with other, conventional geometries. Fig. 2 illustrates the procedure for the four design steps applied to develop the proposed dual-band antenna, namely:

Step-1 (Ant0): In this step, a reference antenna, or Ant0, is a conventional inset-fed CMPA which is designed by assuming that the specified information includes the resonant frequency f_r (in Hz), a dielectric constant ε_r, and the height of the substrate h_{sub} (in cm). Then, the actual radius R (in cm) of the patch is calculated as in [22]:

$$R = \frac{F}{\left\{1+\frac{2h_{sub}}{\pi\varepsilon_r F}\left(\ln\frac{\pi F}{2h_{sub}}+1.7726\right)\right\}^{1/2}} \tag{1a}$$

where

$$F = \frac{8.791\times10^9}{f_r\sqrt{\varepsilon_r}} \tag{1b}$$

By substituting $f_r = 5.8$ GHz, $\varepsilon_r = 4.4$ (FR4), and $h_{sub} = 0.8$ mm in Eq. (1), one can see that $F = 0.7309$ and $R = 0.693$ cm. Then, $R = 6.93$ mm is used as an initial value in designing Ant0, and subsequently CST MWS is performed to fine-tune R, and the other geometric dimensions are optimized to make Ant0 resonate at 5.8 GHz. The final optimized dimensions of Ant0 were set as follows: $R = 7.3$ mm; $L_{sub} = 25$ mm; $W_{sub} = 18$ mm; $h_{sub} = 0.8$ mm; $L_f = 8$ mm; $W_f = 1.6$ mm; $L_s = 5$ mm; and $W_s = 0.5$ mm. Fig. 3 shows the reflection coefficient (S_{11}) curves of the various antennas (Ant0–Ant3). As can be observed from this figure, Ant0 is a single-band antenna that resonates at 5.8 GHz with $S_{11} = -13.25$ dB.

Step-2 (Ant1): This step presents the design of a conventional CPW-fed circular patch antenna (Ant1) to resonate at $f_r = 3.5$ GHz by removing the ground plane in the back side of

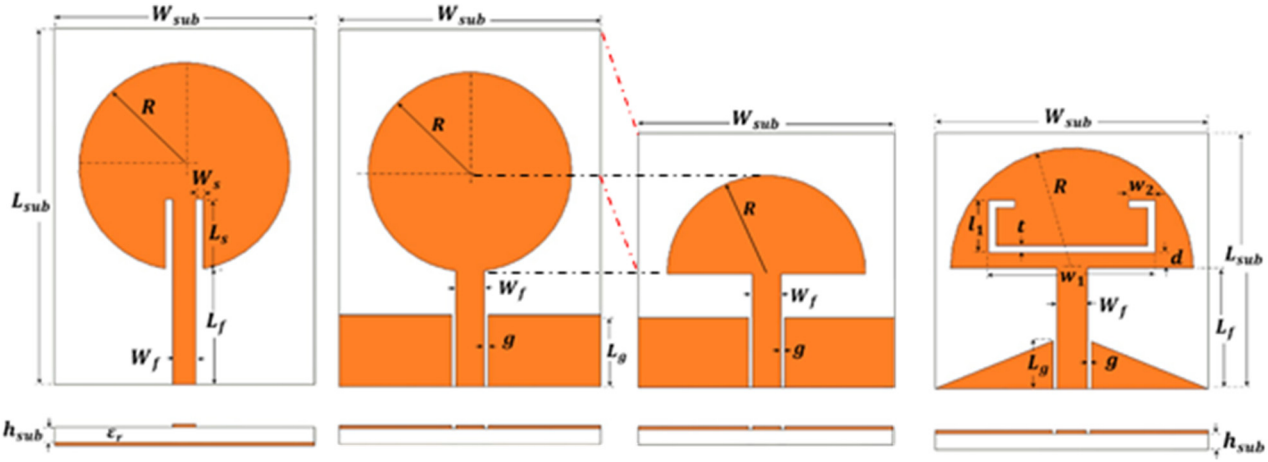

Ant0 Ant1 Ant2 Ant3

Fig. 2. Geometry of various antennas (Ant0–Ant3) involved in the design evolution of the proposed antenna.

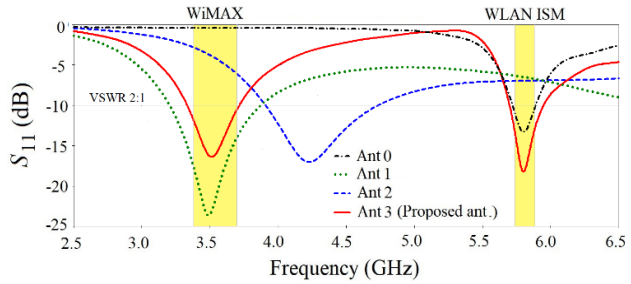

Fig. 3. CST simulated reflection coefficient curves of various antennas (Ant0–Ant3).

Ant0 and placing a pair of ground planes of height $L_g = 5$ mm around the CPW stripline (length $L_f = 8$ mm and width $W_f = 2$ mm) at a distance of $g = 0.25$ mm. The total dimensions $L_{sub} \times W_{sub}$ of Ant1 are the same as those of Ant0 (25 mm × 18 mm). As shown in Fig. 3, Ant1 operates at a 3.5-GHz resonant frequency with −10 dB impedance bandwidth ranging from 3.20 to 3.87 GHz. Thus, Ant1 represents the main designed antenna operating at the desired lower frequency band suitable for a 3.5-GHz application from which the proposed antenna is obtained.

Step-3 (Ant2): In this step, a semi-circular patch antenna (Ant2) is produced by removing the lower half circle of Ant1. Thus, the size of Ant2 ($L_{sub} \times W_{sub}$) is the substrate length $L_{sub} = 17$ mm, which is lower than that of Ant1 by the value of a circular patch radius $R = 7$ mm, and its substrate width W_{sub} is the same as that for Ant1, 18 mm—that is, there is a gain in size reduction of 32%. As shown in Fig. 3, Ant2 resonates at $f_r = 4.23$ GHz. It can be noticed from this figure that the three previously designed antennas (Ant0–Ant2) cover a single band at the following resonant frequencies: 5.8, 3.5, and 4.23 GHz; and thus a modification must be made on Ant2 for possessing a dual-band characteristic.

Step-4 (Ant3): In this fourth and final step of the design procedure, the proposed antenna (Ant3) is obtained by adding a folded U-shaped slot structure on the lower side of the semi-circular patch of Ant2, as shown in Fig. 2. It can be noted from Fig. 3 that the proposed antenna covers the desired bands: 3.5-GHz WiMAX band (3.4–3.7 GHz), and 5.8-GHz WLAN ISM band (5.725–5.875 GHz). The proposed antenna has exquisite features, such as a simple structure, miniaturized dimensions (17 × 18 × 0.8 mm^3), and easy fabrication.

III. Parametric Study and Analysis

In this section, the return loss performance of the proposed dual-band antenna is examined by analyzing its important key geometrical parameters, and interesting conclusions can be drawn from these analyses. These parameters include a half-circle patch radius R, the CPW feedline length L_f, and the ground length L_g, in addition to U-shaped slot parameters (major and minor widths, w_1 and w_2, respectively, the length l_1, the width t, and the distance d, from which the slot is cut from the patch). In order to study the impact of varying the aforementioned parameters on return loss, only one target parameter is varied at a time, whereas all other geometrical parameters retain their same values, as in Table 1.

Figs. 4 and 5 show the impact of the variation of the following geometrical parameters, R, L_f, L_g, and U-shaped slot parameters (w_1, l_1, w_2, d, and t), on the simulated reflection coefficient, respectively. One can notice from these figures that the variation of each of the abovementioned parameters has a different impact on the two resonant modes excited on the antenna, the first and second resonance frequencies, f_r^1 and f_r^2, and their corresponding level of return loss, S_{11}^1 and S_{11}^2, respectively. Table 2 summarizes the effect of these eight parameters on both resonant frequencies, for which the following notation is used: slight increase (↑), strong increase (↑↑), slight decrease (↓), strong decrease (↓↓), and approximately negligible change (−).

It can be seen from Figs. 4(a)–(c) and the three pink-shaded rows in Table 2 for parameters R, L_f, and L_g that f_r^1 of the

Table 2. Simulated influence of geometrical parameters of the antenna on reflection coefficient peak frequencies

Parameter	Variation range (mm)	Step size (mm)	Frequency shift		Reflection coefficient shift	
			f_r^1	f_r^2	S_{11}^1	S_{11}^2
R	7.50–9.00	0.50	↓	↑	↓	↓
L_f	6.00–9.00	1.00	↓	↓	↑	↓↓
L_g	2.00–5.00	1.00	↑	↑	↑	↑
w_1	9.00–12.00	1.00	↓	↓↓	↓	↑
d	0.50–2.00	0.50	↑	↓↓	↑	↑↑
w_2	1.25–2.00	0.25	–	↓	–	–
l_1	2.00–3.50	0.50	–	↓↓	–	–
t	0.25–1.00	0.25	–	↑↑	–	↑↑

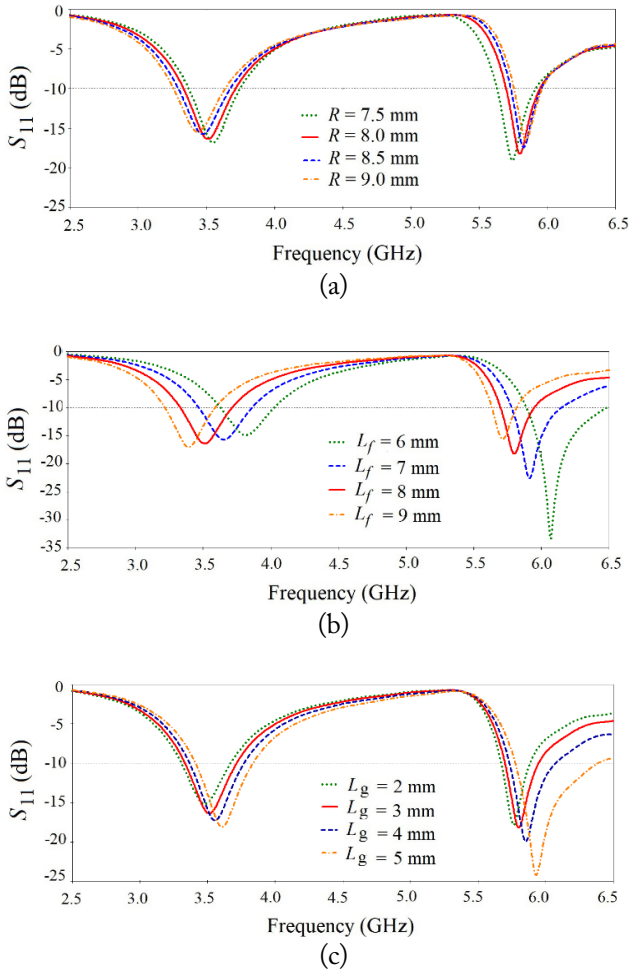

Fig. 4. Impact of varying (a) the half-circle patch, (b) the feed length, and (c) the ground length on the reflection coefficient.

lower band is slightly decreased with increasing R and L_f, and is slightly increased with increasing L_g. Meanwhile, f_r^2 of the higher band is slightly increased with increasing R and L_g, and is slightly decreased with increasing L_f. Thus, there is a slight shifting in both resonance frequencies of the lower and higher band, but with acceptable values of their return losses, S_{11}^1 and S_{11}^2, respectively, when R, L_f, or L_g is varied.

As mentioned earlier, one objective of slot loading is to make the proposed antenna operate on an additional higher-order mode, and it is easily controlled by slot dimensions without affecting the dominant lower resonant mode patch antenna. This concept is investigated by studying the effect of varying U-shaped slot dimensions (w_1, l_1, w_2, t, and d, which are displayed as five green-shaded rows in Table 2) on the reflection coefficient of the proposed antenna. The main idea behind using the proposed slot-loading technique can be clarified with the aid of plotting the surface current distribution at the higher- and lower-order modes of the patch antenna.

It can be observed from Table 2 and Fig. 5(a) that the effect of increasing the major slot width w_1 from 9 to 12 mm f_r^2 (f_r^1) is strongly (slightly) decreased, and its S_{11}^2 (S_{11}^1) is slightly increased (decreased). Fig. 5(b) shows the impact of sweeping the slot distance d from 0.5 to 2 mm on the return loss of the

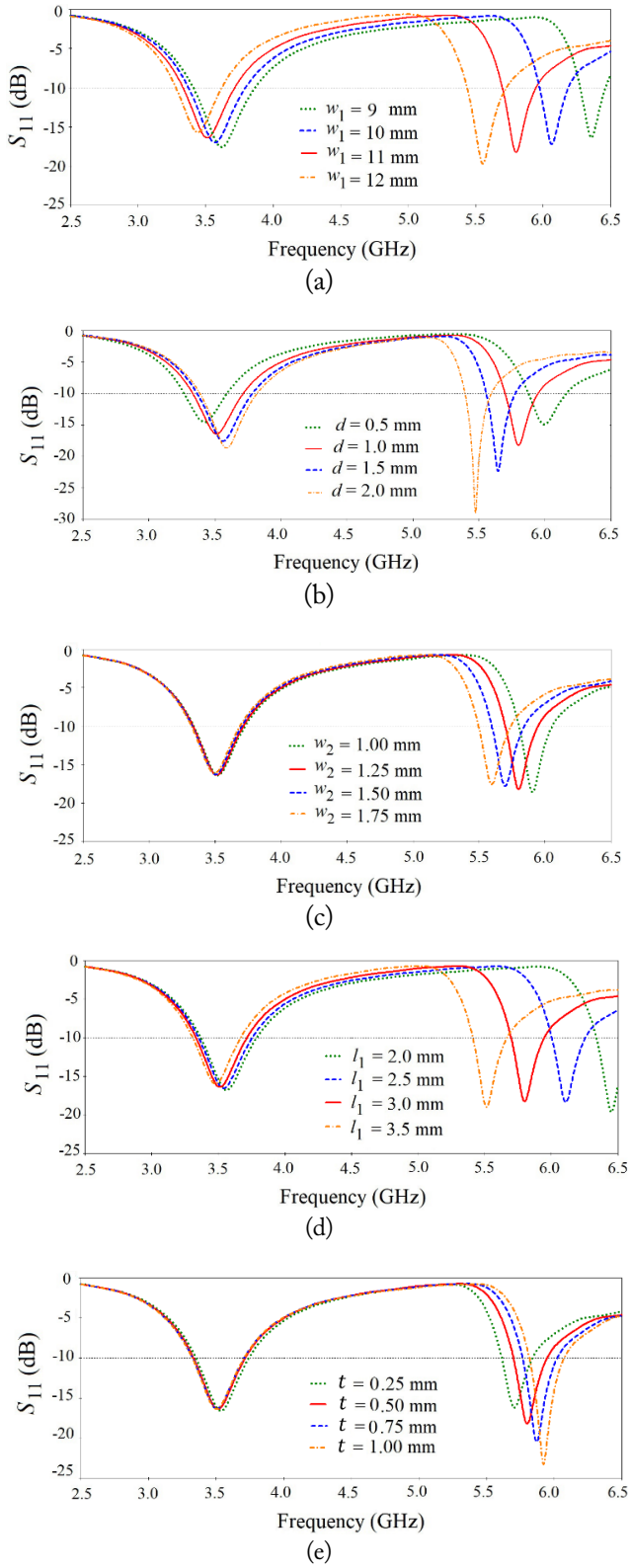

Fig. 5. Impact of sweeping (a) the major width w_1, (b) the distance location d, (c) the minor width w_2, (d) the length l_1, and (e) the thickness t of the U-slot on the reflection coefficient of the proposed antenna.

antenna. It can be seen from this figure that increasing d causes f_r^2 (S_{11}^2) to strongly decrease (increase), whereas both f_r^1 and S_{11}^1 are slightly increased. On the other hand, it can be seen from Fig. 5(c), (d), and (e) that the minor slot width and length, w_2 and l_1, and the thickness t, respectively, play a main role in strongly controlling the shifting of higher resonant frequency f_r^2 without any affect on either the lower resonant frequency f_r^1 or on the peaks of return loss at f_r^1 and f_r^2—that is, S_{11}^1 and S_{11}^2, respectively.

To confirm that the antenna prototype operates over two different frequency bands, Figs. 6 and 7 show the simulated reflection coefficient curves and the surface current distribution on the metallic region for the proposed antenna, with and without a U-slot structure. It can be seen from Fig. 6 that when an antenna is loaded by a U-slot, two resonance frequencies appear in the frequency response; in the case where the U-slot is not used, only one resonance mode is excited by the antenna. As expected, the behavior of the surface current distribution at $f_r^1 = 3.5$ GHz (Fig. 7(a)) significantly differs from that at $f_r^2 = 5.8$ GHz (Fig. 7(b)) when the U-slot is used. As seen from Fig. 7(a), at a low resonant frequency of 3.5 GHz, the maximum current (appearing as a red color) flows from the SMA connector toward the half-circle patch antenna's radiator via the CPW feedline, concentrating around the edges of the U-slot structure.

Thus, the guided wavelength λ_r^1 and the effective path of the current to flow at $f_r^1 = 3.5$ GHz, L_{eff}^1, are calculated as

$$L_{\text{eff}}^1 = L_f + 0.5w_1 + l_1 + w_2 + d \tag{2a}$$

$$\lambda_r^1 = c/f_r^1\sqrt{\epsilon_r} \tag{2b}$$

where c is the speed of light in free space. By substituting in Eq. (2) the specified parameters listed in Table 1, one can get $L_{\text{eff}}^1 \cong 19.25$ mm, which is nearly equal to $\lambda_r^1 = 20.60$ mm.

In the same manner, the surface current at higher resonant frequency $f_r^2 = 5.8$ GHz still flows to the top of the radiating structure (Fig. 7(b)), but it is significantly concentrated (red color) around the edges of the U-slot, moderately distributed (green color) at the CPW stripline, and nearly no current flows (blue color) at the region above the center of the U-slot structure. Thus, the nearest region to the slot structure represents the effective path L_{eff}^2 over which the surface current at $f_r^2 = 5.8$ GHz flows. The value of L_{eff}^2 and the guided wavelength at f_r^2 are calculated as

$$L_{\text{eff}}^2 = 0.5w_1 + l_1 + w_2 \tag{3a}$$

$$\lambda_r^2 = c/f_r^2\sqrt{\epsilon_r} \tag{3b}$$

and from (3), it is found that $L_{\text{eff}}^2 \cong 10.25$ mm, which is close to one-half of λ_r^2—that is, $\lambda_r^2 = 12.45$ mm.

On the other hand, as can be seen from Fig. 7(c) and (d), for the case without using the U-slot structure, there is more current to flow (red color) at the two side edges of the CPW-fed stripline nearer to the resonant frequency 3.5 GHz (Fig. 7(c)), and no current (blue color) flows at 5.8 GHz (Fig. 7(d)). Therefore, it is clear from the previous discussion that inserting proper dimensions of the U-slot structure into the half-circle patch plays a key role for the proposed antenna to operate over the desired DB frequency ranges.

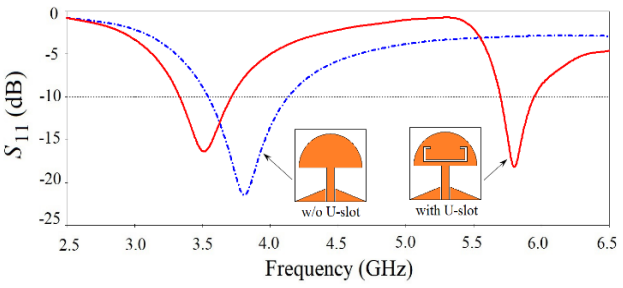

Fig. 6. CST simulated reflection coefficient curves of proposed antenna, with and without the U-slot.

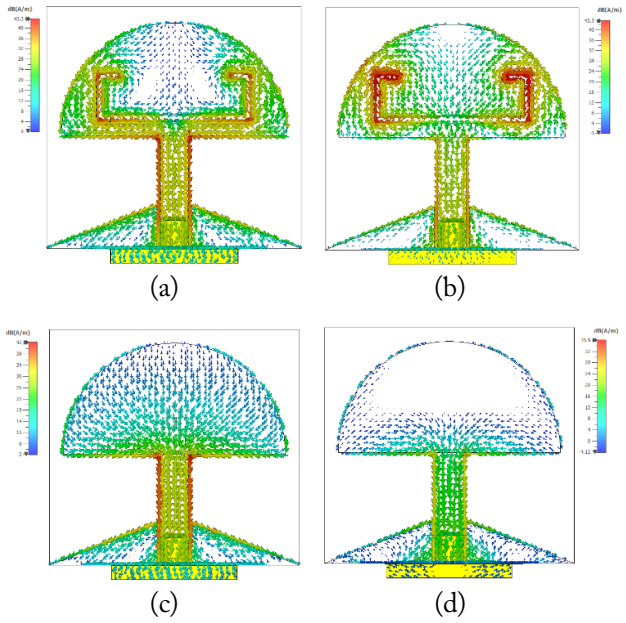

Fig. 7. Simulated surface current distributions for the proposed antenna with a U-slot at (a) 3.5 GHz and (b) 5.8 GHz, and without a U-slot at (c) 3.5 GHz and (d) 5.8 GHz. Red color represents maximum, blue color represents minimum, and green color represents moderate current.

IV. Experimental and Simulated Results and Discussion

In the previous section, the proposed antenna was successfully designed to cover the desired bands using a full-wave CST MWS simulator. In this section, a commercially, widely known software tool—namely, HFSS—is used to validate the simulated

return loss S_{11}, and a measured result of the fabricated prototype is compared with the simulated results. Then, the performance of the antenna, such as far-field characteristics, gain, efficiency, and radiation patterns, using CST and HFSS software is discussed. Finally, a comparison of the proposed antenna with other reported antennas is addressed

1. Reflection Coefficient

To validate the CST and HFSS simulated results in terms of reflection coefficient S_{11}, an optimized version of the prototype designed antenna, with a miniaturized size of 17 × 18 × 0.8 mm^3, was fabricated on an FR4 substrate as shown in Fig. 8. An Agilent/HP N9923A 6 GHz Handheld RF vector network analyzer (VNA) was used for obtaining the measured result. The comparison of the simulated and measured S_{11} of the fabricated antenna is displayed in Fig. 9.

As can be seen from Fig. 9, good agreement between the CST and HFSS simulated results were obtained, and a slightly marginal deviation in these simulated results can be attributed to differences in the numerical methods and boundary conditions used by the two simulator programs. The measured and simulated results are nearly identical over the two operating bands, and the slight difference between them is due to the uncertainty in relative permittivity, heights, and properties of available dielectric materials, or due to inaccuracies in the fabrication process. Table 3 summarizes the simulated and measured frequency bands covered by the antenna in terms of resonant frequency (f_r^1 and f_r^2), lower frequency (f_L^1 and f_L^2), and higher frequency (f_H^1 and f_H^2) for band 1 and band 2, respectively.

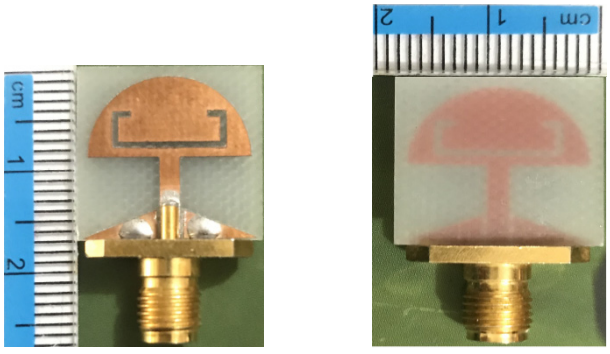

Fig. 8. Prototype of the proposed dual band antenna: (a) front view and (b) back view.

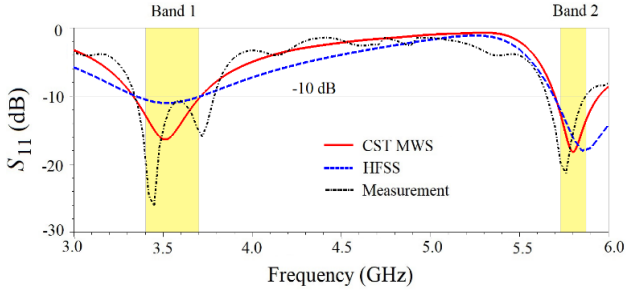

Fig. 9. Comparison of measured and simulated S_{11}.

Table 3. Comparison of the measured and simulated CST MWS and HFSS results of the frequency bands covered by the proposed antenna (unit: GHz)

$\lvert S_{11}\rvert$ (dB)	Band 1			Band 2		
	f_r^1	f_L^1	f_H^1	f_r^2	f_L^2	f_H^2
CST	3.50	3.30	3.71	5.80	5.70	5.94
HFSS	3.50	3.35	3.71	5.85	5.69	>6.00
Measured	3.45	3.33	3.78	5.76	5.65	5.87

It can be observed from Fig. 9 and Table 3 that the simulated band 1 is 3.5 GHz (3.30–3.71 GHz) using CST and 3.5 GHz (3.35–3.71 GHz) using HFSS, whereas the measured band 1 is 3.45 GHz (3.33–3.78 GHz). The simulated band 2 is 5.8 GHz (5.70–5.94 GHz) and 5.86 GHz (5.69–greater than 6 GHz) using CST and HFSS, respectively, and the measured result is 5.76 GHz (5.65–5.87 GHz). Hence, the proposed antenna successfully covers the desired bands required by WiMAX and WLAN systems.

2. Far-field Radiation Performance

Regarding the study of radiation properties, Fig. 10 elucidates the CST (right) and HFSS (left) three-dimensional (3D) simulated gain radiation patterns of the proposed antenna at the resonant frequencies of 3.5 and 5.8 GHz. At both the lower frequency, 3.5 GHz (Fig. 10(a)), and higher frequency, 5.8 GHz (Fig. 10(b)), a radiation pattern close to the conventional monopole antenna pattern is exhibited by the proposed antenna with

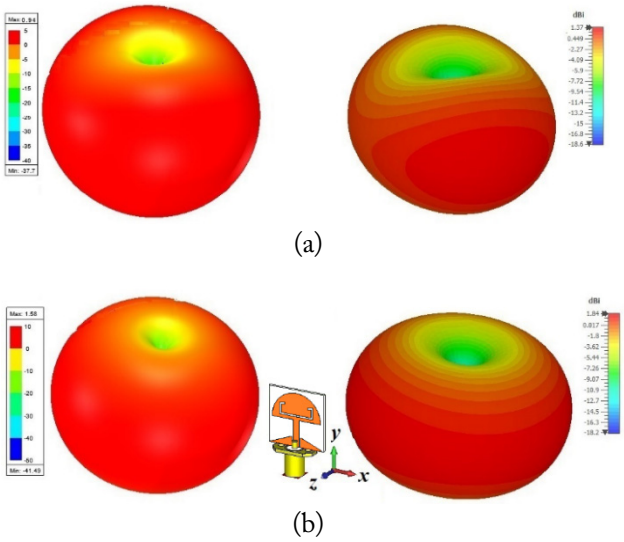

Fig. 10. Comparison between CST (right) and HFSS (left) simulated 3D radiation patterns of the proposed antenna at two frequencies: (a) 3.5 GHz and (b) 5.8 GHz.

an omnidirectional characteristic in the azimuthal (xz-plane or $\phi = 0^{\circ}$), and a butterfly-shaped pattern in the elevation (yz-plane or $\phi = 90^{\circ}$) with null radiation is exhibited along the y-axis. It is clear from this figure that there is good agreement between CST and HFSS simulated results for the 3D radiation patterns of the antenna.

For further validation and comparison purposes, Fig. 11 shows the CST and HFSS simulated two-dimensional (2D) radiation patterns of the antenna at 3.5 and 5.8 GHz in the two fundamental cut planes: E- or xz-pane, and H- or yz-plane.

At the lower frequency (Fig. 11(a)) and higher frequency (Fig. 11(b)), an almost (nearly) similar 2D gain radiation pattern in both the E- and H- planes can be seen, as omnidirectional and figure-eight-shaped pattern behavior, respectively, is observed for the CST and HFSS software. As deduced from the above-mentioned study of the surface current characteristic, the radiation behavior of the prototype antenna further confirms that both the semi-circular patch radiator and the U-shaped slot structure act like a half-wave bipolar at 3.5 and 5.8 GHz. Moreover, the total values of 3D gain achieved from the antenna along the maximum radiation at 3.5 and 5.8 GHz are 1.58 dB (1.84) and 0.94 dB (1.37 dB), respectively, for the HFSS (CST) EM simulator.

3. Realized Gain and Efficiency

The simulated peak realized gain and efficiency for the proposed antenna at both the desired lower and upper frequency bands (3.4–3.7 GHz and 5.725–5.875 GHz) are plotted in Fig. 12. As seen from Fig. 12(a), using CST (HFSS), a maximum gain of 1.83 dB (1.58 dB) and 1.37 dB (0.94 dB) at 3.5 and 5.8 GHz, respectively, is achieved, and the gain ranges in the lower and upper bands are 1.32–1.57 dB (1.12–1.43 dB) and 0.79–1.41 dB (0–1.22 dB). Thus, nearly acceptable results are obtained from the simulated realized gain of the antenna using the CST and HFSS programs.

Fig. 12(b) shows the plot of total efficiency at the desired aforementioned lower and upper frequency bands. As is clear from Fig. 12(b), a maximum efficiency of 94.2% (97.6%) and 79.2% (84.1%) at 3.5 and 5.8 GHz, respectively, is gained, and the ranges of efficiency in the lower and upper bands are 84.6%–87.8% (82.2%–85.6%) and 68.4%–80.9% (82.1%–85.2%) using CST (HFSS).

4. Comparison of Proposed Antenna with Other Reported Antennas

Table 4 provides a comparison between the proposed antenna and some other reported compact dual-band antennas from the open literature. In Tale 4, λ_1 is calculated at the lower frequency in the first band. As can be observed from Table 4, the proposed antenna has a miniaturized size of $A_{\mathrm{Pro}} = 306\ \mathrm{mm}^2$ or $0.0413{\lambda_1}^2$, which is considered the smallest area among the published antennas' areas A_{Pub} listed in Table 4. Hence, a gain in the criterion of relative area A_{r}, which is calculated by dividing A_{Pro} (in ${\lambda_1}^2$) by A_{Pub} (in ${\lambda_1}^2$), results in $A_{\mathrm{r}} = 0.73$ being achieved by the proposed antenna with respect to the smallest area of the reported antenna in literature [10].

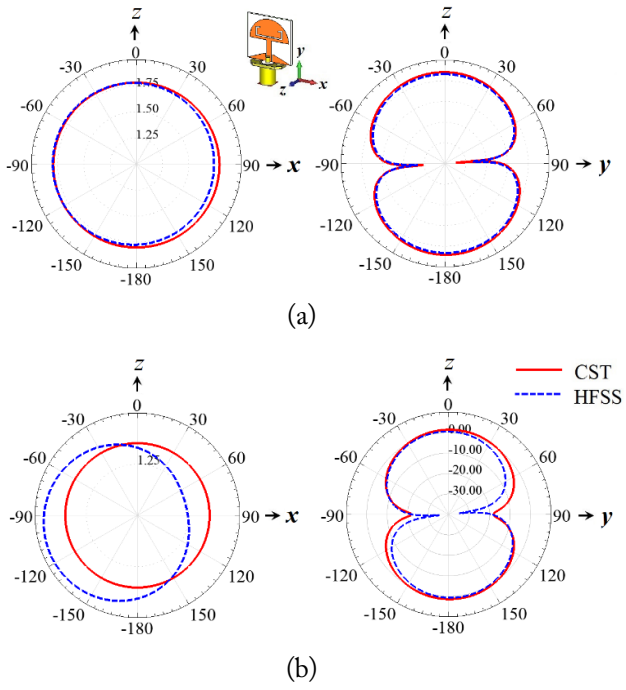

Fig. 11. Comparison between CST and HFSS simulated 2D radiation patterns of the proposed antenna at two frequencies: (a) 3.5 GHz and (b) 5.8 GHz.

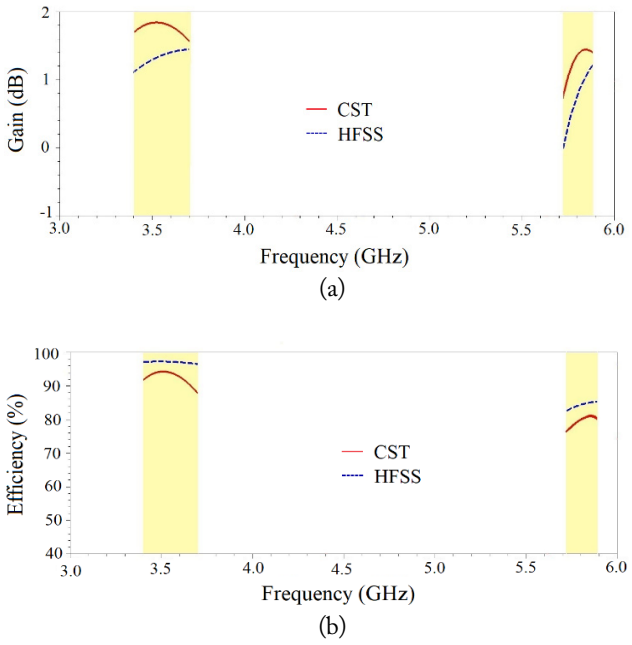

Fig. 12. Comparison between CST and HFSS simulated results: (a) gain and (b) efficiency.

Table 4. A comparison between recent reported dual-band antennas and the proposed antenna

Ref.	Resonant freq. f_{r1} (lower freq.–higher freq.) (GHz)	Antenna type	ε_r	Thickness (mm)	Antenna size ($L_{sub} \times W_{sub}$)	Total area (mm^2)	Total area (λ_1^2) at f_{r1}	Relative area A_r
[9]	2.44 (2.43–2.45) 5.82 (5.72–5.91)	Coupled-fed fan-shaped patch antenna	2.2	1.6	48 × 48	2,304	0.1537	0.27
[10]	2.45 (2.20–2.65) 5.15 (5.0–5.45)	CPW-fed, uniplanar structure	4.4	1.6	25 × 34	850	0.0567	0.73
[11]	2.5 (2.30–4.25) 5.5 (4.95–5.95)	CPW-fed wideband Koch snowflake fractal	4.4	1.0	41.5 × 27.0	1,120	0.0778	0.53
[12]	3.4 (3.12–3.82) 5.5 (5.15–5.83)	CPW-fed, pentagonal ring fractal antenna	4.4	1.6	22 × 22	484	0.0648	0.64
[13]	3.5 (3.05–3.84) 5.5, 6.8 (5.24–7.54)	9-Point-star-shaped monopole	-	-	30 × 45	1,350	0.1780	0.23
[19]	3.5 (3.06–3.89) 5.5 (5.14–5.93)	CPW-fed, two-arm strip with partial ground	4.4	1.6	20 × 22	440	0.0599	0.69
[20]	3.55 (3.36–3.69) 4.8 (4.35–6.00)	CPW-fed, meander folded-shaped monopole	4.4	1.6	21 × 21	441	0.0619	0.67
[21]	2.5 (2.22–2.79) 5.8 (5.42–6.04)	Stripline-fed metamaterial-based folded monopole	4.4	1.6	44 × 70	3,080	0.2139	0.19
This work	3.5 (3.30–3.71) 5.8 (5.70–5.94)	CPW-fed, semi-circular slotted antenna	4.4	0.8	17 × 18	306	0.0417	1

V. Conclusion

A miniaturized CPW-fed SCSA is proposed for operation at 3.5-GHz WiMAX and 5.8-GHz WLAN ISM band systems. A thin folded U-shaped slot structure was employed for generating the higher resonance frequency to cover the 5.8-GHz band. The effects of varying various design parameters on the antenna's frequency bands were comprehensively addressed. A valuable conclusion was drawn from this study that via the proper insertion of an optimized slot structure in the patch, the proposed antenna has the ability to easily generate the second resonant frequency with sufficient bandwidth without affecting the first resonant frequency in the lower band.

The antenna model was designed by using the full-wave CST MWS program, and the simulated results were validated by using the HFSS simulator; good agreement between these results was achieved. The simulated and measured results of the fabricated prototype structure are also in good agreement, confirming that the designed antenna is useful for compact, multi-standard WiMAX and WLAN applications.

The authors would like to thank Dr. Ghassan N. Jawad from the University of Baghdad for providing the measurement results, and Prof. Raad S. Fyath from Al-Nahrain University for his assistance in improving this manuscript.

References

[1] A. A. Jabar and D. K. Naji, "Design of miniaturized quad-band dual-arm spiral patch antenna for RFID, WLAN and WiMAX applications," *Progress In Electromagnetics Research*, vol. 91, pp. 97-113, 2019.

[2] M. A. Abdalla and Z. Hu, "Design and analysis of a compact quad band loaded monopole antenna with independent resonators," *International Journal of Microwave and Wireless Technologies*, vol. 10, no. 4, pp. 479-486, 2018.

[3] M. I. Maricar, A. Bahar, S. Greedy, C. Smartt, S. Phang, G. Gradoni, R. Cross, S. C. Creagh, G. Tanner, and D. W. Thomas, "Design and characterization of a diamond-shaed monopole antenna," *Microwave and Optical Technology Letters*, col. 59, no. 10, pp. 2695-2698, 2017.

[4] D. Fonseca, F. Pereira, and U. R. Vitor, "Study of patch antennas with Koch curve form slots," *Journal of Microwaves, Optoelectronics and Electromagnetic Applications*, vol. 18, no. 3, pp. 399-407, 2019.

[5] M. S. Islam, M. T. Islam, M. A. Ullah, G. K. Beng, N. Amin, and N. Misran, "A modified meander line microstrip patch antenna with enhanced bandwidth for 2.4 GHz ISM-band Internet of Things (IoT) applications," *IEEE Access*, vol. 7, pp. 127850-127861, 2019.

[6] D. K. Naji and A. A. Abdul-Kareem, "A dual-band U-slot PIFA antenna with ground slit for RFID applications,"

Journal of Emerging Trends in Computing and Information Sciences, vol. 4, no. 2, pp. 213-220, 2013.

[7] Y. C. Chen and M. Z. Weng, "Triple-band L-shaped monopole antenna with defected ground plane for WLAN and WiMAX application" *Journal of Electronic Science and Technology*, vol. 13, no. 2, pp. 135-138, 2015.

[8] S. P. Gangwar, K. Gangwar, and A. Kumar, "Dual band modified circular ring shaped slot antenna for GSM and WiMAX applications," *Microwave and Optical Technology Letters*, vol. 61, no. 12, pp. 2752-2759, 2019.

[9] J. Tak, D. G. Kang, and J. Choi, "A compact dual-band monopolar patch antenna using TM01 and TM41 moes," *Microwave and Optical Technology Letters*, vol. 58, no. 7, pp. 1699-1703, 2016.

[10] G. Singla, R. Khanna, and D. Parkash, "CPW fed rectangular rings-based patch antenna with DGS for WLAN/ NII applications," *International Journal of Microwave and Wireless Technologies*, vol. 11, no. 5-6, pp. 523-531, 2019.

[11] D. Li, F. S. Zhang, Z. N. Zhao, L. T. Ma, and X. N. Li, "A CPW-fed wideband Koch snowflake fractal monopole for WLAN/WiMAX applications," *Progress In Electromagnetics Research C*, vol. 28, pp. 143-153, 2012.

[12] D. K. Naji, "Compact design of dual-band fractal ring antenna for WiMAX and WLAN applications," *International Journal of Electromagnetics and Applications*, vol. 6, no. 2, pp. 42-50, 2016.

[13] T. Mandal and S. Das, "Coplanar waveguide fed 9-point star shape monopole antennas for worldwide interoperability for microwave access and wireless local area network applications," *The Journal of Engineering*, vol. 2014, no. 4, pp. 155-160, 2014.

[14] J. H. Yoon, S. J. Ha, and Y. C. Rhee, "A novel monopole antenna with two arc-shaped strips for WLAN/WiMAX application," *Journal of Electromagnetic Engineering and Science*, vol. 15, no. 1, pp. 6-13, 2015.

[15] J. H. Yoon, D. S. Im, S. J. Ha, and Y. C. Rhee, "A circular-ring monopole antenna with a half-circular ring and grund slot for WLAN/WiMAX triple-band operations," *Journal of Electromagnetic Engineering and Sciene*, vol. 14, no. 4, pp. 367-375, 2014.

[16] H. Liu, P. Wen, S. Zhu, B. Ren, X. Guan, and H. Yu, "Quad-band CPW-fed monopole antenna based on flexible pentangle-loop radiator," *IEEE Antennas and Wireless Propagation Letters*, vol. 14, pp. 1373-1376, 2015.

[17] A. A. Omar, O. Abu Safia, and M. Nedil, "UWB coplanar waveguide-fed coplanar strips rectangular spiral antenna," *International Journal of RF and Microwave Computer-Aided Engineering*, vol. 27, no. 7, article no. e21115, 2017.

[18] A. A. Jabar and D. K. Naji, "Optimization design methodology of miniaturized five-band antenna for RFID, GSM, and WiMAX applications," *Progress in Electromagnetics Research*, vol. 83, pp. 177-201, 2019.

[19] H. Taghizadeh, C. Ghobadi, B. Azarm, and M. Majidzadeh, "Grounded coplanar waveguide-fed compact MIMO antenna for wireless portable applications," *Radioengineering*, vol. 28, no. 3, pp. 528-534, 2019.

[20] D. K. Naji, "Design of compact dual-band and tri-band microstrip patch antennas," *International Journal of Electromagnetics and Applications*, vol. 8, pp. 26-34, 2018.

[21] H. Li, Q. Zheng, J. Ding, and G. Guo, "Dual-band planar antenna loaded with CRLH unit cell for WLAN/ iMAX application," *IET Microwaves, Antennas & Propagation*, vol. 12, no. 1, pp. 132-136, 2018.

[22] C. A. Balanis, *Antenna Theory: Analysis and Design*. Hoboken, NJ: John Wiley & Sons, 2016.

Dhirgham Kamal Naji

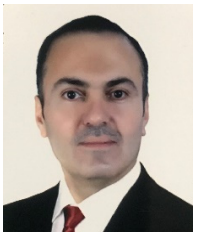

received a B.S. in Electrical Engineering from Baghdad University in 1995, an M.Sc. degree in Communications Engineering from Baghdad University, Baghdad, Iraq, in 1998, and a Ph.D. degree in Modern Communications Engineering from Al-Nahrain University, Baghdad, Iraq, in 2013. His fields of research include fractal antennas, RFID antenna miniaturization, and electromagnetic optimization.